2017 IEEE/RSJ International Conference on Intelligent Robots and Systems (IROS)
September 24–28, 2017, Vancouver, BC, Canada

# Design and Implementation of Multirotor Aerial-Underwater Vehicles with Experimental Results*

Marco M. Maia[1], Diego A. Mercado[1] and F. Javier Diez[1]

*Abstract*— **Design and implementation of a fully-working multirotor Unmanned Aerial-Underwater Vehicle (UAUV) was successfully accomplished in the present work. The proposed prototype consists of a multirotor vehicle in an octo-quadcopter configuration, which is well suited for good transition between mediums. The mathematical model is provided by means of the Newton-Euler formalism, highlighting the impact of the drastic change in density on the vehicle dynamics. A hierarchical controller is employed for attitude tracking, utilizing a proportional control law in cascade with a body angular rate Proportional-Integral-Derivative (PID) controller. Altitude stabilization is achieved by a PID controller with compensation of the restoring forces, while a gain scheduling strategy handles the change of medium. Furthermore, the proposed platform was extensively tested in simulations and real-time experiments under real conditions, with promising results in both mediums, and seamless transition between them.**

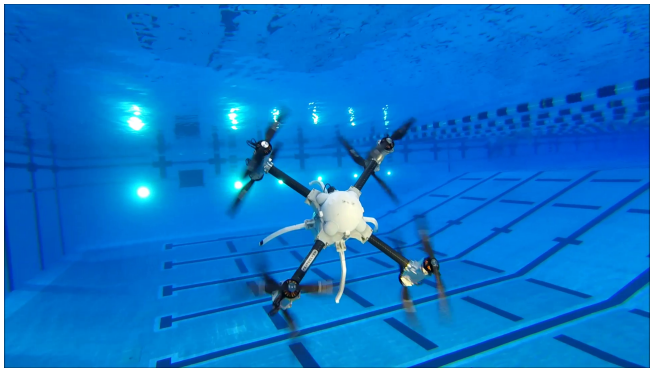

Fig. 1: Photograph of the Naviator conducting a fully autonomous mission (untethered) of a "Figure 8" maneuver, with transition out of the water, as seen in the video at `https://youtu.be/V-QRaZpx8CU`

## I. Introduction

There have been great strides in the development of unmanned systems in recent years, particularly with regard to Unmanned Aerial Vehicles (UAV) as it is a sector that has exciting applications and could benefit from a variety of improvements. Another segment that has seen an abundance of innovation recently is Unmanned Underwater Vehicles (UUV). But they are normally studied separately and designed with high degree of specialization to the corresponding medium.

Bridging the efforts made in UAV and UUV to present a vehicle that is capable of both aerial and underwater navigation is of optimal interest. Benefits comprise of rapid deployment for both air/underwater missions (ie. search/rescue), point-to-point underwater (UW) mapping and object recognition without needing to consistantly overcome opposite water currents. Such a vehicle would also serve as a multipurpose extreme weather vehicle, since it would be completely waterproof, perfectly adapted for rain, and recoverable by air if driven into a body of water. Thus, it is not surprising to note that this subject is not new but a revisited one, as it was tried in the past, at least conceptually, by the Soviet Union [1] during the last world war and has been of interest to DARPA in the last decade [2]. Unfortunately, however, former approaches to the issue were far too costly or impractical to be of any real use.

Of the many unmanned aerial systems, one type drawing special attention is of the multirotor class, due to its robustness, reliability and practicality. Multirotors are vertical take-off and landing vehicles (VTOL) that do not require variable pitch propulsion systems and although under-actuated, can easily compensate for irregular mass concentrations of payload. Research efforts in this area include improving the vehicle control strategy and optimizing the system while trying different multirotor configurations [3]. As the UAV market expands together with new well-defined regulations, the industry has begun to join the race, which has led to smarter and more reliable vehicles. After all, if they are to be commercialized, they must be capable of safely interacting with other people and objects alike.

The underwater research community also has a favorite, the Remotely Operated underwater Vehicles (ROV), which have been in use since the 1950s and are still used today [4]. One novelty as of late with regard to UUV has been the development of autonomous underwater vehicles capable of long term deployment, chiefly for data collection and underwater mapping. Underwater gliders have done well in achieving this objective, with some gliders capable of operations lasting over one year [5].

Unmanned aerial-underwater systems are a new class of unmanned vehicles with limitless possibilities. Efforts have been made to merge the capabilities of aerial and underwater systems, such as the AquaMAV that dives into the water [6]. Other approaches include submersible airplanes [7], [8] and launching an UAV out of the water [9], [10], but without the possibility of vehicle retrieval.

A multirotor vehicle in the octa-quadcopter configuration comprised of a single type of propellers equally adept at

*This work was supported by Office of Naval Research (ONR), Grant No. N00014-15-2235 with Dr. Thomas McKenna serving as Program Manager.

[1]Authors are with Department of Mechanical and Aerospace Engineering Rutgers, the State University of New Jersey. 98 Brett Road, Piscataway, NJ 08854-8058. `diez@rutgers.edu`

operating in air and underwater is presented in this work—the ”Naviator”. This novel air-underwater platform is capable of seamlessly transitioning through the air-water interface and operating equally well in both air and underwater. We have found that coaxial multirotor vehicles are well suited for transitioning out of the water due to the fact that while some rotors are at the air-water interface, where it is difficult to achieve reliable propulsion, there are always enough rotors working continuously in one of the mediums to provide thrust and attitude control. A vehicle concept that utilizes a similar multirotor configuration is presented in [11], [12], employing aerial rotors on the top and underwater rotors on the bottom, but no prototype was developed. Unfortunately, in such a configuration the underwater rotors and respective components would be of little use during air flight, thus becoming payload.

To our knowledge, the Naviator is the first vehicle of its kind that has successfully proven itself to be reliable and effective in both air and underwater operation in real field tests (see Fig. 1). The custom firmware developed for the autopilot and speed controllers allow for full control over rotor angular velocities and enables the vehicle to be extremely precise and agile. This work is the first to present experimental data on this platform capabilities as it pertains to underwater maneuverability.

One of the major challenges that arise from utilizing a predominantly aerial or underwater platform for use in opposite environments (ie. from air to water or water to air) is in adapting its existing control strategy for the intended medium due to their bias toward stability and performance. For instance, aerial vehicles such as multirotors often pose a limit on their lean angles to ensure stable flight. As such, the topic of this paper will be to re-purpose the controls of a popular multirotor autopilot firmware for dual operation in the air and underwater. We will validate our multi-medium vehicle with simulations and a real-time experiment.

The paper is structured as follows: Section II will introduce the Naviator prototype, Section III will present the dynamical model used for the system, while Section IV will describe the control strategy employed. Next, Section V will study the findings from the numerical simulations and Section VI will discuss the results obtained from the real-time experiment. To conclude, Section VII will present the generalized results and discuss their meaning and implications.

## II. The Naviator Platform

The challenge in having a multi-medium vehicle that can operate within multiple mediums is in transitioning seamlessly between them, even when subjected to harsh conditions. In order to achieve this, the propulsion system of the Naviator must first be capable of operating continuously at any given time in spite of the medium in which it is in. Toward this goal, the octa-quadcopter configuration (X8) is employed, which is a multirotor much like a quadcopter, but with each arm comprising of a counter-rotating coaxial pair of rotors, as depicted in Fig. 2. An optimal vertical distance

Fig. 2: Picture of the actual Naviator platform.

between the coaxial pair is selected to facilitate transition. In truth, any number of arms can be used without changing originality. However, the X8 configuration is a convenient choice due to its symmetry. Due to the difference in rotor operational speeds between mediums such as air and water, it is best to avoid thrust generation at the interface since the potentially chaotic thrust generation there might impair the ability of the vehicle to maintain control. In the case of transitioning out of the water, the procedure is as depicted in Fig. 3, where the only instances that a rotor is reliably providing thrust is when it is not at the air-water interface. Moreover, this configuration is adequate for operation in the surface and transitions in more challenging conditions, such as wavy environments, where the vehicle could adapt to the inclination of the surface and transition out. In order to guarantee the proper transition between mediums, it is imperative to sense the medium in which the rotors are immersed. Hence, two water sensors were added to the vehicle at the top and the bottom of the vessel.

Other challenges stem from needing to protect sensitive electronics from water while allowing for heat dissipation, avoiding complexity and reducing added weight. The heat dissipation issue is resolved through the use of lightweight aluminum enclosures, which together with the central plastic pressure vessel, form an impenetrable seal that is designed to withstand several meters of water depth, although through

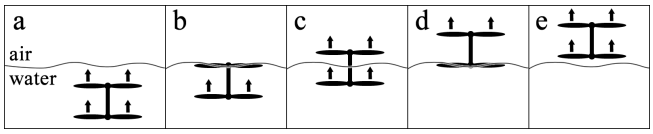


Fig. 3: Graphical depiction of the Naviator transition out of water strategy for a single coaxial rotor assembly where the wavy line is the air-water interface showing (a) both of the rotors providing thrust in water, (b) the top rotor at the interface and the bottom rotor providing thrust in water, (c) the top rotor providing thrust in air and the bottom rotor providing thrust in water, (d) the top rotor providing thrust in the air and the bottom rotor at the interface and (e) both of the rotors providing thrust in air.

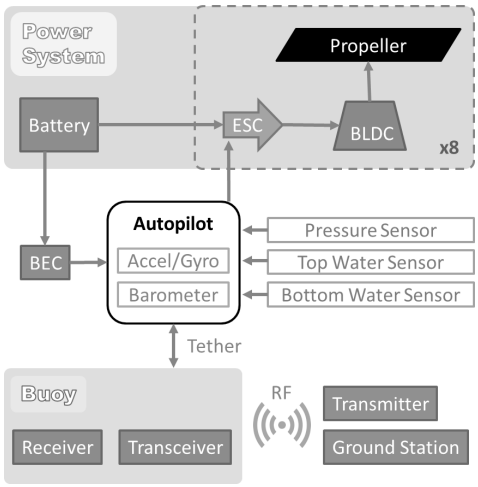


Fig. 4: Naviator platform overview.

careful selection of materials, the depth could be greatly extended.

There are several advantages that come with operating in a denser medium. In mediums with enough density (ie. water), it is easy to design the vehicle to be neutrally buoyant if so desired, where the buoyancy force acting upward cancels the weight acting downward. The outcome is a multirotor vehicle that no longer has to compensate for its most power hungry force—its weight. Ideally, such a system could remain at fixed depth indefinitely without utilizing energy. In practice, however, due to energy lost from battery self-discharge and energy drawn from idling and safety components, the vehicle could be dormant for years at a time. In our case, we opted to have the Naviator be negatively buoyant and so it has underwater weight, although this could be easily changed at any time.

The power bank of the vehicle is entirely within the pressure vessel. Communication is achieved both wirelessly through radio frequency (RF) and an optional tether for telemetry communication and manual control. The tether connects from the vehicle to a floating buoy that is towed as necessary, limiting only the depth that the vehicle can travel, but not translational motion. We have utilized tethers of up to 30$m$ in field tests and it is mainly used as a debugging tool. An open-source multirotor unmanned aerial vehicle firmware created by the drones community (ArduCopter) is used as a baseline and then heavily customized to support underwater operation as well as autonomous underwater missions. The motor drivers (ESC) for the brushless motors (BLDC) used also contain custom firmware that allow the rotors to spin fast when in air and slowly when underwater (slower by two orders of magnitude). An overview of the main components of the system is presented in Fig. 4.

## III. Dynamical Model

The dynamic model was obtained using the Newton-Euler formalism and the resulting laws of motion are outlined in (1)-(4) (see for example [13], [14]). The inertial frame axis are defined as $\hat{\mathbf{i}}$, $\hat{\mathbf{j}}$, and $\hat{\mathbf{k}}$ and the body frame axis are defined as $\hat{\mathbf{e}}_1$, $\hat{\mathbf{e}}_2$, and $\hat{\mathbf{e}}_3$ for the x, y and z axis, respectively (see Fig. 5).

$$\dot{\mathbf{r}} = \mathbf{v} \tag{1}$$

$$m\dot{\mathbf{v}} = T_\Sigma \mathbf{R}(\Phi)\hat{\mathbf{e}}_3 - g(m - \rho V)\hat{\mathbf{k}} - \mathbf{F_{Dr}}(\mathbf{R_e}, \mathbf{v}, \rho) \tag{2}$$

$$\omega = \mathbf{Q}\dot{\Phi} \tag{3}$$

$$\mathbf{J}\dot{\omega} = -\omega \times \mathbf{J}\omega - \mathbf{F_{D\Phi}}(\mathbf{R_e}, \omega, \rho) + \tau \tag{4}$$

In the dynamic equations, $T_\Sigma$ is the total thrust produced by all the rotors, $\mathbf{R}(\Phi)$ is the rotation matrix from inertial to body frame coordinates, $\hat{\mathbf{e}}_3 = [0,0,1]^{\mathrm{T}}$ is a unit vector, $g$ is the acceleration due to gravity, $m$ is the mass of the vehicle, $\rho$ is the density of the medium, $V$ is the volume of the vehicle, $\mathbf{v}$ is the vehicle velocity, $\omega$ is the angular velocity of the vehicle in the body frame, $\dot{\omega}$ is the angular acceleration of the vehicle in the body frame, $\Phi$ is the Euler angle vector, $\dot{\Phi}$ is the Euler angle rate vector, $\mathbf{Q}$ is a matrix that transforms the Euler angle rates to body angular rates, $\mathbf{J}$ is the mass moment of inertia matrix for the entire vehicle and $\tau$ are the input torques. The Reynolds number $\mathbf{R_e}$ is defined in (5) where $\mu$ is the dynamic viscosity of the fluid medium.

$$\mathbf{R_e} = \frac{\rho \mathbf{v} \mathbf{D}}{\mu} \tag{5}$$

The drag components for the vehicle translational drag force $\mathbf{F_{Dr}}$ and vehicle rotational drag torque $\mathbf{F_{D\Phi}}$ are defined in (6) and (7). Although the drag coefficients and characteristic areas vary with the angles of attack, speed and fluid properties, we will model them as a single coefficient and area for simplicity. The translational drag force is due to the linear velocities $\mathbf{v}$ and the rotational drag torque is due to the angular velocity of a sphere rotating with $\omega$ about its origin [15] plus the moments induced by drag of the arms modeled at the rotors.

$$\mathbf{F_{Dr}} = \frac{1}{2}\rho \mathbf{A_r} \mathbf{C_{Dr}}(\mathbf{R_e}) \mathbf{v} \circ \mathbf{v} \circ \frac{\mathbf{v}}{\| \mathbf{v} \|} \tag{6}$$

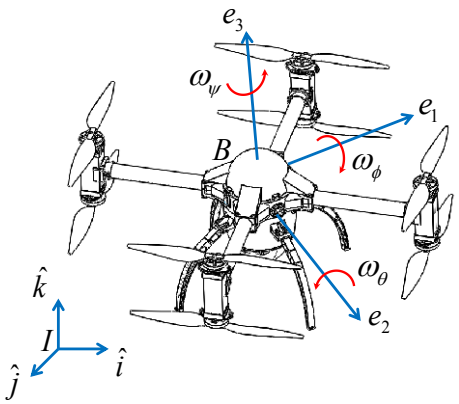


Fig. 5: Unmanned Aerial-Underwater Vehicle coordinate frames.

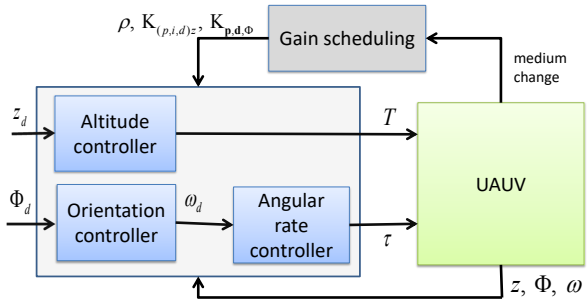


Fig. 6: Control strategy block diagram.

$$\mathbf{F_{D\Phi}} = 4 \cdot \frac{1}{2}\rho \mathbf{A_\Phi} \mathbf{C_{D\Phi}}(\mathbf{R_e})\omega L \circ \omega L \circ \frac{\omega}{\| \omega \|} + 8\pi R_\Phi^3 \mu \omega \quad (7)$$

In the drag force and drag torque, $\circ$ is the Hadamard product (also known as element/entry-wise multiplication), $\mathbf{A_r}$ is the characteristic area of the entire vehicle, $\mathbf{A_\Phi}$ is the characteristic area of the vehicle arms modeled at the rotors, $\mathbf{C_{Dr}}$ is the drag coefficient for translation, $\mathbf{C_{D\Phi}}$ is the drag coefficient for the arms modeled at the rotors, $L$ is the arm length from the center of the vehicle to the rotor and $R_\Phi$ is the radius of the vehicle pressure vessel spherical representation. The thrust forces and countertorques are given by (8) and (9) below:

$$\begin{bmatrix} T_\Sigma \\ \tau \end{bmatrix} = \begin{bmatrix} 1 & 1 & 1 & 1 & 1 & 1 & 1 & 1 \\ -l & l & l & -l & l & -l & -l & l \\ l & l & -l & -l & l & l & -l & -l \\ -b & b & -b & b & b & -b & b & -b \end{bmatrix} \begin{bmatrix} T_1 \\ \vdots \\ T_8 \end{bmatrix} \quad (8)$$

$$T_i = K_{T_j} \rho \varpi_\mathbf{i}{}^T \varpi_\mathbf{i} \quad (9)$$

where $i$ is the rotor index, $j \in \{A : air, W : water, \dots\}$ is the medium index, $\varpi_i$ is the angular speed of the rotor, $T_i$ is the thrust produced by the rotor $i$, $l$ is the arm length used for the pitch/roll and $b = K_{QT}$ is a conversion factor from thrust to countertorque.

## IV. Control Scheme

Multirotor vehicles are a kind of underactuated systems with only four inputs $\mathbf{u} = [T \ \tau]^T$ (full torque actuation and a single force direction) and six outputs $[\mathbf{r} \ \Phi]^T$. Henceforth, only four outputs are directly actuated ($\Phi$, $z$), while the two remaining states, i.e. the horizontal position ($x$, $y$), are highly coupled with the vehicle orientation. We consider the problem of designing a control strategy to stabilize the vehicle's attitude and altitude to their desired reference values $\Phi_d$, $z_d$. The resulting control law should be adequate for both mediums.

First of all, let us define the altitude error $\tilde{z}$ as

$$\tilde{z} = z - z_d \quad (10)$$

and the orientation error $\tilde{\Phi}$ as

$$\tilde{\Phi} = \Phi - \Phi_d \quad (11)$$

Then, we select a PID controller with compensation of the restoring forces as follows

$$T = \frac{g(m - V\rho) - K_{pz}\tilde{z} - K_{dz}\dot{\tilde{z}} - K_{iz}\int \tilde{z} dt}{\hat{\mathbf{e}}_3^T \mathbf{R}(\Phi)\hat{\mathbf{e}}_3} \quad (12)$$

As for the attitude stabilization, we propose a hierarchical controller with an outer proportional orientation feedback in cascade with an inner PID angular body rate controller, such that the desired angular rate $\omega_d$ is used as a virtual input to drive the vehicle's orientation $\Phi$ to its desired reference, while the input torques $\tau$ are used to control the angular rates $\omega$, i.e.

$$\tilde{\omega} = \omega + \mathbf{Q}\mathbf{K}_\Phi \tilde{\Phi} \quad (13)$$

$$\tau = -\mathbf{K_p}\tilde{\omega} - \mathbf{K_d}\dot{\tilde{\omega}} - \mathbf{K_i}\int \tilde{\omega} dt \quad (14)$$

The control gains $K_{pz}$, $K_{dz}$, $K_{iz}$, $\mathbf{K_p}$, $\mathbf{K_d}$, $\mathbf{K_i}$ and $\mathbf{K}_\Phi$ are constant for a constant medium, but may differ for different mediums. This control strategy is well suited for easy implementation on commercial autopilots.

Finally, a gain scheduling [16] takes care of the dramatic change of density between mediums. This kind of adaptive controller updates the system parameters according to known varying conditions. This is the case of Unmanned Aerial-Underwater Vehicles (UAUV) where the medium density is well known for both air and water, and the medium change can be easily detected using one or more water sensors. Adequate control parameters can also be updated according to the corresponding medium. Fig. 6 depicts a block diagram of the overall control architecture.

## V. Numerical Simulations

The simulations were carried out using MATLAB Simulink® employing the hierarchical approach described in Section IV with an Euler angle reference controller that feeds into a body angular rate reference controller. The physical properties of the simulation were chosen to match the prototype, as described in Table I. When the control strategy was implemented, the autopilot firmware and Simulink® setup were made to have the same control scheme with equivalent gains. These gains were selected in simulation and tunned experimentally, and are presented in Table II.

TABLE I: Naviator Physical Properties

| Mass $[kg]$ | Volume $[cm^3]$ | Inertia $\times 10^{-3}$ |
|---|---|---|
| 3.85 | 3630 | [69.01,69.24,118.96] |
| $K_{T_A}\left[\frac{N \cdot m^3 \cdot s^2}{kg \cdot rad^2}\right]$ | $K_{T_W}\left[\frac{N \cdot m^3 \cdot s^2}{kg \cdot rad^2}\right]$ | $K_{QT}[m]$ |
| $2.45 \cdot 10^{-7}$ | $2.55 \cdot 10^{-7}$ | 0.0205 |

TABLE II: Control gains underwater

| $K_{pz}$ | $K_{dz}$, $K_{iz}$ | $\mathbf{K}_\Phi$ |
|---|---|---|
| 5 | 0 | 4.5 |
| $\mathbf{K_p}$ | $\mathbf{K_d} \times 10^{-3}$ | $\mathbf{K_i}$ |
| $diag(0.25, 0.25, 0.2)$ | $diag(4, 4, 10)$ | $diag(0.01, 0.01, 0)$ |

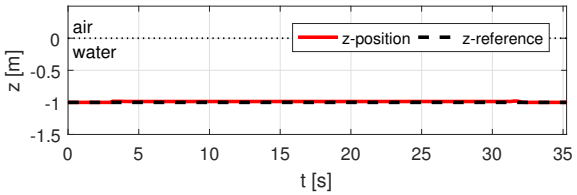


Fig. 7: Euler angles and respective input reference angles of the vehicle over time as it conducts a figure 8 maneuver in simulation.

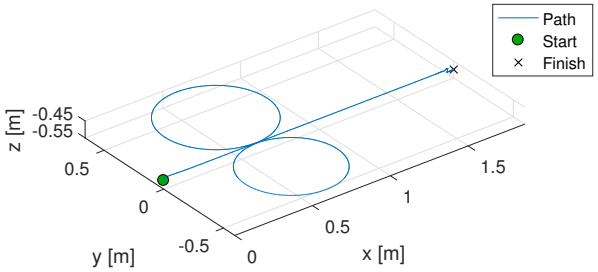


Fig. 9: Position of the vehicle over time as it conducts a figure 8 maneuver in simulation.

In order to validate that the control strategy employing gain scheduling works for underwater operation, we begin by running an underwater simulation with underwater gains. A mission that highlights the excellent maneuverability of the prototype is in conducting a "Figure 8" shape underwater. We have feedback on the altitude/depth and attitude of the vehicle. Therefore, we can complete a figure eight by commanding the vehicle pitch forward and translate while maintaining depth to make a full right-hand turn followed by a full left hand turn and we can control the turn radius by modifying increasing or decreasing the desired yaw, which translates to prescribing a yaw rate (but in the form of a linear yaw angle reference). Throughout the simulation, the vehicle will be given an altitude reference of -1$m$ (ie. in water) and a roll angle of 0°. During this, the vehicle will be told to pitch forward to 75° and then complete the right and left hand turns. The turns will be provided as a linear yaw input from 0° to 360° and then back to 0°, after which the vehicle will pitch to level back to 0° and the mission will conclude. Figures 7 and 8 show the altitude and Euler angles, respectively.

The altitude controller shown in Fig. 7 has excellent agreement with the desired reference, even with the drastic forward pitch angle of 75°. The Euler angles shown in Fig. 8 also match with the reference very well. A small perturbation can be seen in the roll as the vehicle conducts a drastic yaw change, as seen in 7s, 16s and 25s. The pitch response was great and is able to achieve its target within one second, despite needing to overcome the induced drag torque. The yaw heading of the vehicle is wrapped within -180° to 180° for simplicity and also follows the reference very well, lagging behind by only 0.5s chiefly due to the drags involved.

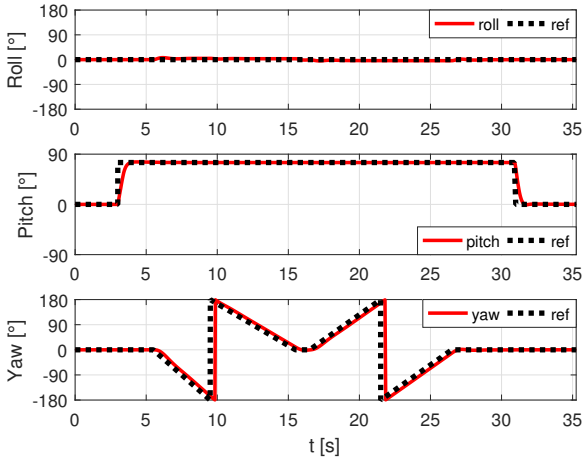


Fig. 8: Euler angles and respective input reference angles of the vehicle over time as it conducts a figure 8 maneuver in simulation.

The output position of the system is shown in Fig. 9 and is a "Figure 8" as expected. One thing to note is that the left-hand turn circle of the path is larger than the right-hand turn. That is because when making the left-hand turn, the vehicle must compensate for both moment of inertia of the platform and angular momentum of the right-hand turn, where as in the right-hand turn there is only the moment of inertia (since linear momentum does not greatly impact the angular rate).

## VI. Real-Time Experiments

The simulation results were validated through several real-time experiments in both mediums. As a proof of concept and in order to highlight the great maneuverability of the proposed configuration, we performed a "Figure 8" mission as the one described in Section V, where the desired references were identical for both. The Naviator was fully autonomous—the references were fed to the vehicle as an input before the mission and later initialized.

The agreement between the outputs and references of altitude in Fig. 11 and Euler angles in Fig. 10 are satisfactory, but there are some errors in altitude and attitude. An offset in the altitude of roughly 1$m$ exists. The optional tether was used to aide in data collection and the weight and pull of the tether is known to adversely affect the weight compensation of the vehicle, and so, an offset is expected. The coupling between the Euler angle changes are more pronounced than in the simulation, but the trends are the same—whenever there is a large change in the yaw angle, there is a perturbation in the roll. The drop in pitch angle during turns when the yaw rate is constant indicates that the proportional gain on the pitch should be increased and favored over the others since it is taken to its extreme.

Given the simplified nature of the dynamic model, the vehicle performed the mission exceptionally well and a

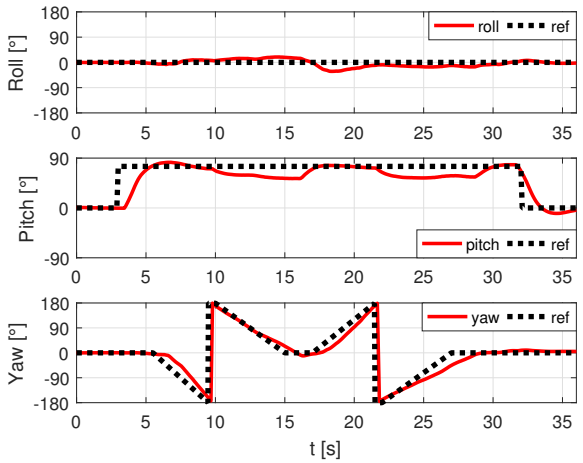


Fig. 10: Euler angles and respective input reference angles of the vehicle over time as it conducts a figure 8 maneuver in the field.

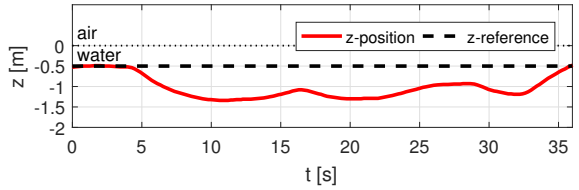


Fig. 11: Altidude/Depth and respective input altitude reference of the vehicle over time as it conducts a figure 8 maneuver in the field.

video of the experiment can be found online at `https://youtu.be/CFioBkh9haQ`. Another video without a tether in which both an autonomous "Figure 8" maneuver and manual transition out of the water are conducted can be found at `https://youtu.be/V-QRaZpx8CU`. In the latter video, we can also appreciate the ability of the vehicle to operate in the interface if necessary.

## VII. Conclusions and Perspectives

A fully functional prototype was developed which is capable of operating equally well in the air and underwater. A system model was presented for a multi-medium vehicle and a control strategy was applied that emcompasses the angle/angle-rate controllers commonly found in commercially available aerial multirotors. Next, a simulation demonstrated that the controller is suitable to drive the vehicle to a desired reference quickly and with little error, despite operating much closer to the Euler angle singularity than typical multirotors. The Naviator platform was introduced as a suitable multi-medium vehicle. Then, the implementation was further validated through a real-time experiment of the same mission as in the simulation, employing equivalent gains, control scheme and control inputs, and the results were satisfactory.

Multi-medium vehicles are an existing new paradigm in robotics with endless possibilities. There still remains much to be done in the subject matter, such as improving the control strategies, multi-medium swarming, sensor fusion, air-underwater communication and more. Nevertheless, multirotors work very well in the air and here, it has been proven that one such system (the Naviator) operates equally well in air as it does underwater. Furthermore, it is capable of transitioning seamlessly between air and water fluid mediums.

## References


[1] G. Petrov. "Flying submarine". In *Journal of fleet*, 1995.

[2] "Broad Agency Announcement: Submersible Aircraft," DARPA, DARPA-BAA-09-06, 2008.

[3] V. Kumar and N. Michael. "Opportunities and challenges with autonomous micro aerial vehicles". In *International Symposium on Robotics Research*, Flagstaff, AZ, 2011.

[4] Robert Bogue. "Underwater robots: a review of technologies and applications", Industrial Robot: An International Journal, Vol. 42 Iss: 3, pp.186 - 191, 2015.

[5] S. Wood. "Autonomous underwater gliders". In *Underwater Vehicles*, Chapter 26, edited by A. V. Inzartsev, 499-524, In-Tech, Vienna, Austria. 2009.

[6] R. Siddall and M. Kova, "Launching the AquaMAV: bioinspired design for aerialaquatic robotic platforms," Bioinsp. Biomim., vol. 9, no. 3, 2014.

[7] A. Fabian, Y. Feng, E. Swartz, D. Thurmer and R. Wang. "Hybrid Aerial Underwater Vehicle (MIT Lincoln Lab)". *SCOPE Projects*, 2012.

[8] D. Edwards. "Flimmer: a Flying Submarine". *Naval Research Laboratory Spectra*, pp. 6-9, 2014.

[9] Kollmorgen, "Sea Sentry Organic Submarine Launched UAV," Kollmorgen Corporation, Radford, 2009.

[10] D. Majumdar, "U.S. Navy Launches UAV from a Submarine," U.S. Naval Institute News, 2013.

[11] P. Drews-Jr, A. Neto and M. Campos. "Hybrid unmanned aerial underwater vehicle: modeling and simulation". In *International Conference on Intelligent Robots and Systems (IROS)*, Chicago, USA, 2014.

[12] A. Neto, L. Mozelli, P. Drews-Jr & M. Campos. "Attitude control for an hybrid unmanned aerial underwater vehicle: a rubust switched strategy with global stability". In *International Conference on Robotics and Automation (ICRA)*, Stockholm, Sweden, 2016.

[13] J. Roskam. "Airplane flight dynamics and automatic flight controls". *Roskam Aviation and Engineering Corporation*, USA, 1982.

[14] T. Fossen. "Guidance and control of ocean vehicles". *John Wiley and sons*, England, 1994.

[15] Lei, U., Yang, C.Y., Wu, K.C., 2006. "Viscous torque on a sphere under arbitrary rotation". *Appl. Phys. Lett.* 89.

[16] Astrom, K. and Wittenmark, B. "Adaptive control". *Addisson-Wesley* 2nd edition, ch. 9, pp. 390-417, USA, 1995.